The current issue and full text archive of this journal is available at
http://www.emerald-library.com

Received January 1999
Revised August 1999
Accepted August 1999

Numerical solutions of the Navier-Stokes and energy equations for laminar incompressible flow past parabolic bodies

O.M. Haddad, M. Abu-Qudais and A.M. Maqableh
Mechanical Engineering Department, Jordan University of Science and Technology, Irbid, Jordan

Keywords *Forced convection, Laminar flow, Numerical solutions*

Abstract *Numerical solutions are presented for steady two-dimensional symmetric flow past parabolic bodies in a uniform stream parallel to its axis. For this study, the full Navier-Stokes equations and energy equation in parabolic coordinates were solved. A second order accurate finite difference scheme on a non-uniform grid was used. The solution domain does not exclude the leading edge region as it is usually done with boundary layer flows. A wide range of Reynolds number* (Re) *is studied for different values of Prandtl number* (Pr). *It is found that the average Nusselt number* ($\overline{Nu}$) *increases as* (Pr) *increases meanwhile,* ($\overline{Nu}$) *decreases with the increase in* (Re).

Nomenclature

a = nose radius of curvature
C_f = skin friction coefficient
D = reference length used to define the Nusselt number
f = modified stream function
g = modified vorticity
h = modified temperature
h_o = convection heat transfer coefficient
i = numerical index in streamwise direction
i_{buf} = the index i at the beginning of the buffer zone
j = numerical index in the wall normal direction
Nu = Nusselt number
$\overline{Nu}$ = average Nusselt number
P = non-dimensional pressure
Pr = Prandtl number
Re = Reynolds number based on the nose radius of curvature
Re_x = Reynolds number based on the local x-coordinate
Re_L = Reynolds number based on ξ_{max}
T = temperature
U_∞ = free-stream velocity
(u,v) = velocity components in the (x,y) directions, respectively
(x,y) = Cartesian coordinates

Greek symbols
θ = non-dimensional temperature
ν = kinematic viscosity
(ξ, η) = parabolic coordinates
ρ = fluid density
ψ = stream function
ω = vorticity

Superscripts
* = dimensional quantity

1. Introduction

With the advent of fast computers, numerical solutions to the full Navier-Stokes (N-S) equations are now possible using various numerical techniques. Up to now, analytical studies of the flow over parabolic cylinders have been

International Journal of Numerical Methods for Heat & Fluid Flow, Vol. 10 No. 1, 2000, pp. 80-93.
© MCB University Press, 0961-5539

restricted to the hydrodynamic part of the problem. Van De Vooren and Dijkstra (1970) have obtained a numerical solution to the N-S equations for laminar incompressible flow past a semi-infinite flat plate. Later the numerical method of solution has been improved by Botta and Dijkstra (1970). A common feature of these studies is the use of parabolic coordinates which are known to be optimal for the flat plate. Also Davis (1967) has studied the laminar flow past a semi-infinite flat plate using parabolic coordinates. In his study, Davis used a series truncation method in which the stream function is locally expanded in a power series in the x-coordinate.

The natural extension of the flat-plate to other body shapes is the parabolic body. Botta *et al.* (1972) have numerically solved the N-S equations for laminar incompressible flow past a parabolic cylinder. Dennis and Walsh (1971) obtained a numerical solution for the steady symmetric viscous flow past a parabolic cylinder in a uniform stream. They obtained a solution using two-dimensional finite difference approximations to the partial differential equations for the stream function and vorticity. Their solutions cover the range of Reynolds number (based on the nose radius of the cylinder) from 0.25 to ∞. Davis (1972) has considered the symmetric laminar incompressible flow past a parabolic cylinder. Davis numerically solved the N-S equations in stream function and vorticity using an alternating direction implicit (ADI) method. Careful attention was focused on extracting singularities from the problem in the limit as Reynolds number goes to zero, and the study covered all values of Reynolds number. Finally, Haddad (1995) and Haddad and Corke (1998) have considered the receptivity of the boundary layer over parabolic bodies to freestream acoustic wave. The flow over a parabola was one part (the basic state) of the solution.

To the authors' best knowledge, there exists no previous study which deals with the energy equation of the flow over parabolic bodies. The purpose of this study is to investigate the forced convection laminar heat transfer characteristics of the flow over parabolic bodies. For this purpose, the energy equation as well as the Navier-Stokes equations are solved numerically. The governing partial differential equations, in stream function, vorticity and temperature, have been finite differenced on a non-uniform grid. Results are presented for both the hydrodynamic and thermal parts of the problem.

2. Formulation of the problem

2.1 Governing equations

Figure 1 shows a schematic diagram for flow problem under consideration. Let the infinite parabolic cylinder be given by the equation

$$x(y) = \frac{1}{2a}(y^2 - a^2) \tag{1}$$

where a is recognized as the nose radius of curvature.

For steady laminar incompressible fluid flow with constant thermophysical properties, the non-dimensional N-S equations and energy equation in

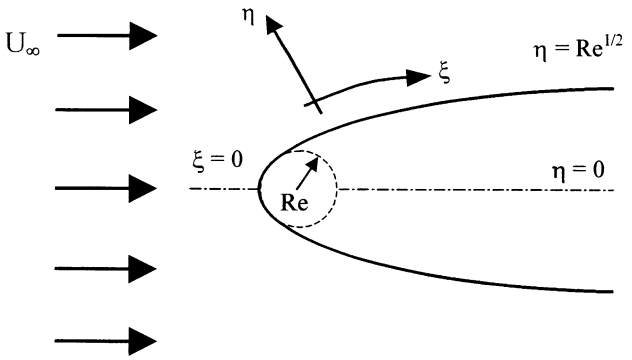

Figure 1.
Schematic diagram for a parabolic body in a uniform stream

parabolic coordinates take the form

$$\frac{\partial^2\psi}{\partial\xi^2}+\frac{\partial^2\psi}{\partial\eta^2}=-\left(\xi^2+\eta^2\right)\omega \tag{2}$$

$$\frac{\partial^2\omega}{\partial\xi^2}+\frac{\partial^2\omega}{\partial\eta^2}+\frac{\partial\psi}{\partial\xi}\frac{\partial\omega}{\partial\eta}-\frac{\partial\psi}{\partial\eta}\frac{\partial\omega}{\partial\xi}=0 \tag{3}$$

$$\frac{1}{Pr}\left(\frac{\partial^2\theta}{\partial\xi^2}+\frac{\partial^2\theta}{\partial\eta^2}\right)+\frac{\partial\psi}{\partial\xi}\frac{\partial\theta}{\partial\eta}-\frac{\partial\psi}{\partial\eta}\frac{\partial\theta}{\partial\xi}=0 \tag{4}$$

where the following set of variables have been introduced to non-dimensionalize the variables:

$$x=\frac{x^*}{(\nu/U_\infty)} \qquad y=\frac{y^*}{(\nu/U_\infty)} \qquad \omega=\frac{\omega^*}{\left(U_\infty^2/\nu\right)}$$
$$\psi=\frac{\psi^*}{\nu} \qquad \theta=\frac{T^*-T_\infty^*}{T_w^*-T_\infty^*} \tag{5}$$

In addition, the parabolic coordinates (ξ,η) are related to the Cartesian coordinates (x,y) by

$$(x+iy)=\frac{(\xi+i\eta)^2}{2} \tag{6}$$

Therefore, the surface of the parabola is located at $\eta_w=Re^{1/2}$, where Re is the Reynolds number based on the nose radius of curvature and $i=\sqrt{-1}$.

In order to remove the singularity at the leading edge of the flat plate, we follow Davis (1972) and introduce the new variables f, g and h where

$$\psi=\xi f(\xi,\eta), \quad \omega=-\frac{\xi}{(\xi^2+\eta^2)}g(\xi,\eta), \quad \theta=-\frac{\xi}{(\xi^2+\eta^2)}h(\xi,\eta) \tag{7}$$

The new dependent variables are then governed by the following equations

$$f_{\eta\eta} - g + f_{\xi\xi} + \frac{2}{\xi} f_{\xi} = 0 \tag{8}$$

$$g_{\eta\eta} + \left(f + \xi f_{\xi} - \frac{4\eta}{\xi^2 + \eta^2} \right) g_{\eta} + \left(\frac{\xi^2 - \eta^2}{\xi^2 + \eta^2} f_{\eta} - \frac{2\eta}{\xi^2 + \eta^2} \left(f + \xi f_{\xi} \right) \right) g - \xi g_{\xi} \left(f_{\eta} + \frac{4}{\xi^2 + \eta^2} \right) + g_{\xi\xi} + \frac{2}{\xi} g_{\xi} = 0 \tag{9}$$

$$h_{\eta\eta} + \left(Pr\left(f + \xi f_{\xi} \right) - \frac{4\eta}{\xi^2 + \eta^2} \right) h_{\eta} + Pr \left(\frac{\xi^2 - \eta^2}{\xi^2 + \eta^2} f_{\eta} - \frac{2\eta}{\xi^2 + \eta^2} \left(f + \xi f_{\xi} \right) \right) h - \xi h_{\xi} \left(Pr f_{\eta} + \frac{4}{\xi^2 + \eta^2} \right) + h_{\xi\xi} + \frac{2}{\xi} h_{\xi} = 0 \tag{10}$$

These equations are changed from elliptic to parabolic when the last two terms in each equation are neglected. This fact had been exploited by Davis (1972) to formulate an efficient numerical solution.

In order to evaluate the pressure on the parabolic surface, we apply the x-momentum equation at the surface and then change the Cartesian variables (x,y) to parabolic variables (ξ,η) to get

$$\frac{\partial p}{\partial \xi} = -\frac{\partial \omega}{\partial \eta} \tag{11}$$

$$= \frac{\xi}{\xi^2 + \eta^2} \left[\frac{\partial g}{\partial \eta} - \frac{2\eta}{\xi^2 + \eta^2} g \right] \tag{12}$$

Following Davis (1972), we introduce the following transformation to remove the singularity from the pressure expression at the leading edge of the flat plate

$$P = p - \frac{\eta}{(\xi^2 + \eta^2)} g(0, Re^{1/2}) \tag{13}$$

Thus

$$\frac{\partial P}{\partial \xi} = \frac{\xi}{\xi^2 + \eta^2} \left[\frac{\partial g}{\partial \eta} - \frac{2\eta}{\xi^2 + \eta^2} (g - g_o) \right] \tag{14}$$

where $g_o = g(0, Re^{1/2})$.

The local skin friction coefficient is given by

$$C_f = \frac{\tau_w^*}{\rho U_\infty^2} = \frac{\partial^2 \psi}{\partial y^2}|_w \tag{15}$$

Applying the stream function equation at the wall yields

$$\frac{\partial^2 \psi}{\partial y^2}|_w = -\omega \tag{16}$$

Therefore

$$\begin{aligned} C_f &= -\omega|_w \\ &= \frac{\xi}{(\xi^2 + Re)} g(\xi, Re^{1/2}) \end{aligned} \tag{17}$$

Finally, the local Nusselt number is defined as

$$Nu = \frac{h_o D^*}{k} \tag{18}$$

where h_o is the convective heat transfer coefficient which is given by

$$h_o = \frac{k}{(T_w^* - T_\infty^*)} \frac{\partial T^*}{\partial y^*}|_w \tag{19}$$

Therefore, by non-dimensionalizing the variables and taking the length $D = \xi_{max}$,

$$Nu(\xi) = \xi_{max} \frac{\partial \theta}{\partial y}|_w \tag{20}$$

and in parabolic variables

$$Nu(\xi) = \frac{\xi \xi_{max}}{\left(\xi^2 + \eta_w^2\right)^2} \left(\xi h_\eta + \eta_w h_\xi\right) - \frac{\eta_w \xi_{max} \left(3\xi^2 - \eta_w^2\right)}{\left(\xi^2 + \eta_w^2\right)^3} h \tag{21}$$

2.2 Boundary conditions

At the wall, we assume the no-slip, no-penetration boundary conditions. In addition, the stream function equation was applied at the wall to get a boundary condition on the wall vorticity, and the surface is assumed to be isothermal. That is

$$\text{at } \eta = Re^{1/2}: \; f = 0, \; \frac{\partial f}{\partial \eta} = 0, \; g = f_{\eta\eta} \text{ and } h = 1 \tag{22}$$

At the freestream, potential flow conditions are prevailing. In addition, we assume isothermal freestream. That is

$$\text{as } \eta \to \infty: \; \frac{\partial f}{\partial \eta} \to 1, \; g \to 0 \text{ and } h \to 0 \tag{23}$$

3. Numerical method of solution

The governing equations are finite differenced using a second order accurate finite difference scheme on a non-uniform grid. A uniform grid was first generated and then Robert's stretching transformation (Anderson *et al.*, 1984) was applied in both streamwise and wall normal direction in order to cluster more points near the leading edge in one direction and near the wall in the other direction. The governing equations were linearized using Newton's linearization technique. Three points central differences were used whenever possible (interior points) otherwise backward or forward differences were used as applicable (boundary points). The resulting system of linear algebraic equations was solved simultaneously by iteration using the proper LINPACK subroutines with the coefficient matrix being of the banded matrix type. More details on the numerical method are given by Maqableh (1997). In general, the solution required seven iterations to converge with a max local iteration error $\leq 10^{-5}$. Solutions are obtained using the digital unix (alpha processor) workstation.

It is worthy of mention here that it is necessary to reduce the number of boundary conditions at the wall from four to three. This was accomplished by finite differentiation of the first two of these boundary conditions, then substituting one equation into the other, thereby the two boundary conditions are; set into one equation. In addition, one should note that the numerical plane must be finite in both streamwise and wall normal direction. It is well-known that for a parabolic cylinder the flow proceeds without separation from stagnation point flow at the nose to Blasius flow farther downstream. Based on the study made by Haddad (1995) and Haddad and Corke (1998), the freestream is located at a distance from the wall that is equivalent to ten times the downstream Blasius boundary layer thickness on a flat plate of the same length as the parabola. Also, in the streamwise direction, the outflow boundary is located at a distance from the leading edge far enough for the Blasius flow to be valid.

Davis (1972) had argued that excluding the elliptic terms (the last two terms) in each of the governing equations results in equations which contain both the first order boundary layer terms and the terms for the second order curvature correction. Based on this, the boundary conditions at the outflow are derived by applying the governing equations at the outflow with the elliptic terms being dropped out. This treatment has the advantage that we are not imposing any solution at downstream infinity (e.g. Blasius solution); nevertheless, we can still compare our solution with the flat plate Blasius solution to validate our approach. To implement this, a buffer zone was specified in which the elliptic terms in the governing equations have been multiplied by a weighting factor, s. The weighting factor was a function of streamwise location only. At the beginning of the buffer zone, $s = 1$. At the end of the buffer zone which corresponds to the outflow boundary, $s = 0$. To smoothly transition from 1 to 0, the weighting factor was given the following form

$$s(i) = \frac{1 + \tanh(arg)}{2} \tag{24}$$

where

$$arg = 4\left\{1 - \frac{2(i - ibuf)}{(Imax - ibuf)}\right\} \tag{25}$$

where i is the numerical index in the streamwise direction and $ibuf$ is the index i at the beginning of the buffer-zone.

4. Results and discussion

4.1 Solution independency

Numerical test calculations were carried out to evaluate the effect of grid size (i.e. number of grid points) on the obtained solution. Attention was focused on the wall vorticity to judge the solution sensitivity. It was found that the numerical results are more sensitive to the number of grid points in the wall normal direction (J_{max}) than in the streamwise direction (I_{max}). Almost identical results were obtained for the cases with $I_{max} = 150$ and $I_{max} = 350$ whereas significant change in the solution has occurred when J_{max} is changed from 30 to 33. The solution was invariant for $J_{max} > 33; thusagridsizeof 200\times 36 pointswasusedthroughoutthisstudy$.

4.2 Pressure distribution

Using the pressure at downstream infinity as a boundary condition, the surface's pressure can be found by integrating from downstream infinity back along the surface.

Equation (14) was integrated using the trapezoidal rule. The results of the integration for different cases of Reynolds number are shown in Figure 2. It can be seen that the pressure gradient everywhere is favourable and the local pressure at the nose increases with Reynolds number. The results are in excellent agreement with those of Davis (1972).

4.3 Skin friction distribution

Skin friction distribution over parabolas at various Reynolds numbers are shown in Figure 3. These distributions are qualitatively similar to the pressure distributions in Figure 2. It can be noted that the more blunt the body, the larger is the local skin friction, with the maximum value being at the leading edge. Obviously, our results agree very well with those of Davis (1972).

4.4 Velocity distribution

Velocity profiles normal to the wall at different stations on the parabolic surface are obtained for different values of Re. In all cases, these profiles develop into a Blasius profile away from the leading edge, as expected. This fact is clearly observed in Figure 4 where one of the velocity profiles far

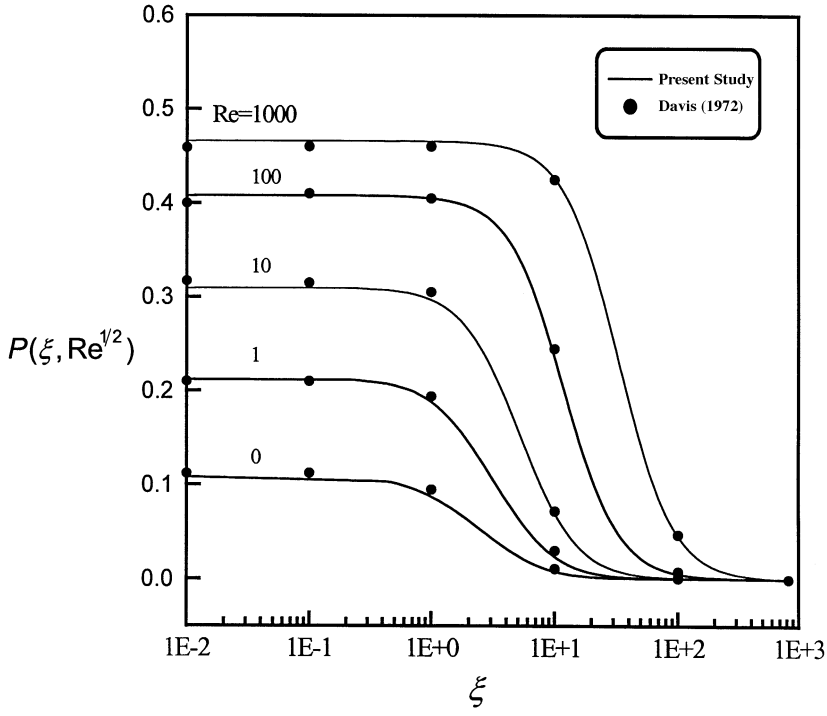

Figure 2.
Pressure distribution on a parabolic body

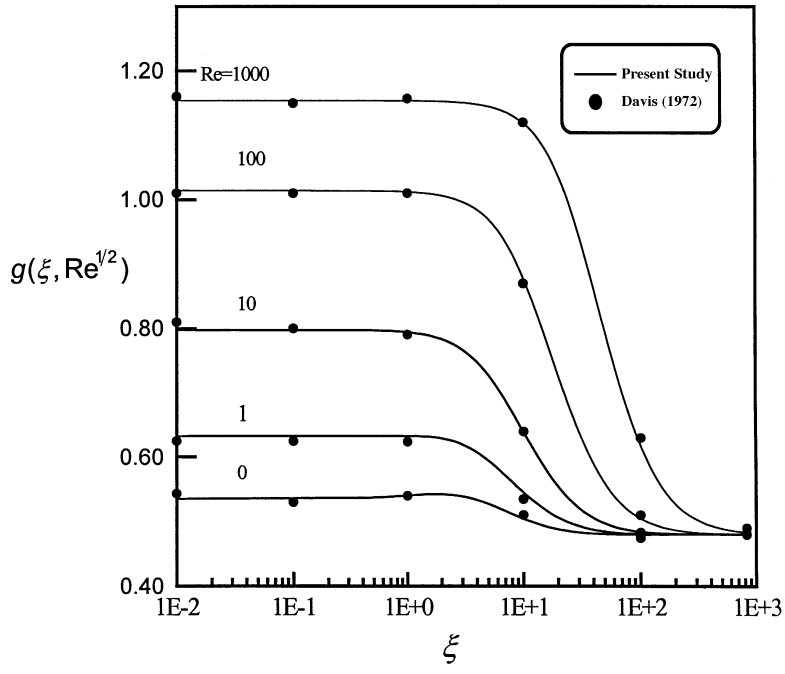

Figure 3.
Skin friction distribution on a parabolic body

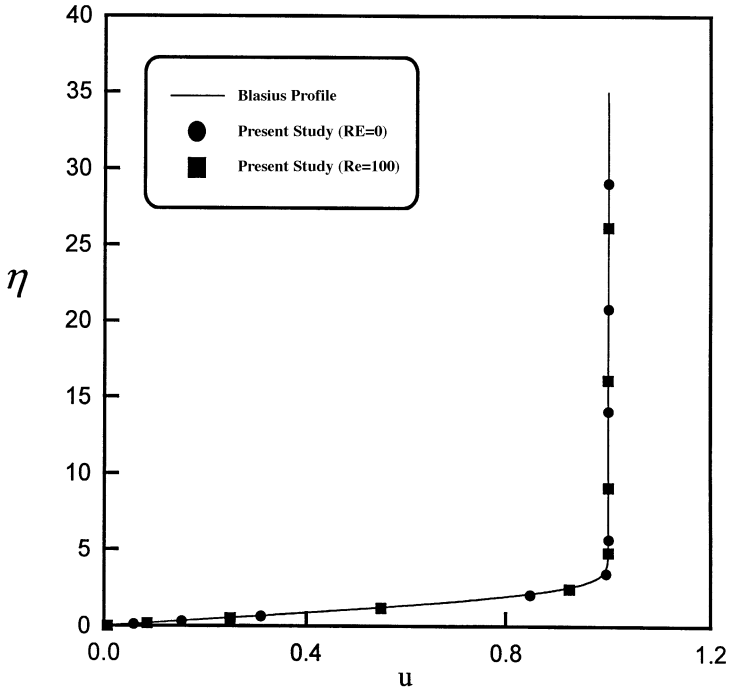

Figure 4.
Comparison of downstream velocity profile with Blasius profile

downstream is compared with Blasius profile for the cases $Re = 0$ (flat plate) and $Re = 100$ (parabolic cylinder). This figure clearly shows that these profiles are identical.

To see the effect of Re on the downstream distance, measured from the leading edge, required by the flow to develop into Blasius flow, the location of the first velocity profile (expressed as $\xi_{Blasius}$) which matches the Blasius profile was plotted versus Re. The result is shown in Figure 5 where it can be seen that the flow required to travel farther downstream away from the leading edge in order to develop into Blasius flow as Reynolds number is increased.

4.5 Temperature distribution

Temperature profiles normal to the wall at different stations on the parabolic surface are obtained for different values of Re. To validate our results for the thermal part of the problem, the temperature profile of the flow over flat plate ($Re = 0$) and away from the leading edge is compared with those presented by Schlichting (1979) for different values of Prandtl number. The comparison is shown in Figure 6 where it can be seen that the agreement is excellent.

4.6 Nusselt number distribution

We first consider the case of flat plate ($Re = 0$) where the effect of Prandtl number on Nusselt number distribution is shown in Figure 7. These distributions have similar trends in that they start with a maximum value at

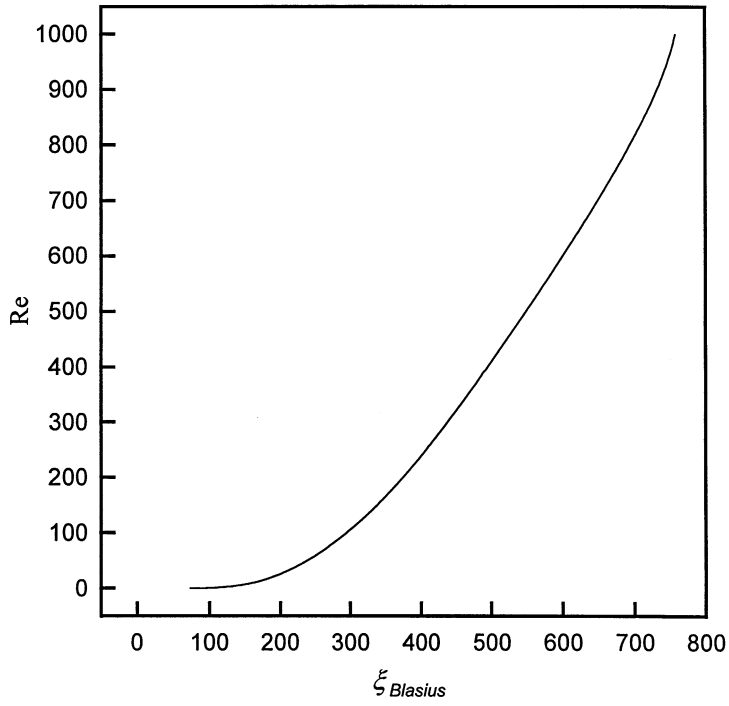

Figure 5.
Effect of bluntness on the first Blasius profile location

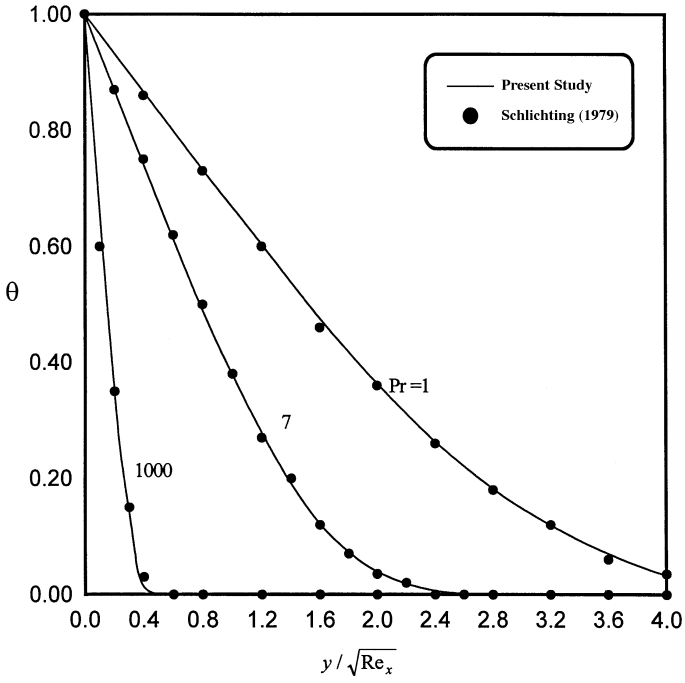

Figure 6.
Downstream temperature profiles at different (Pr)

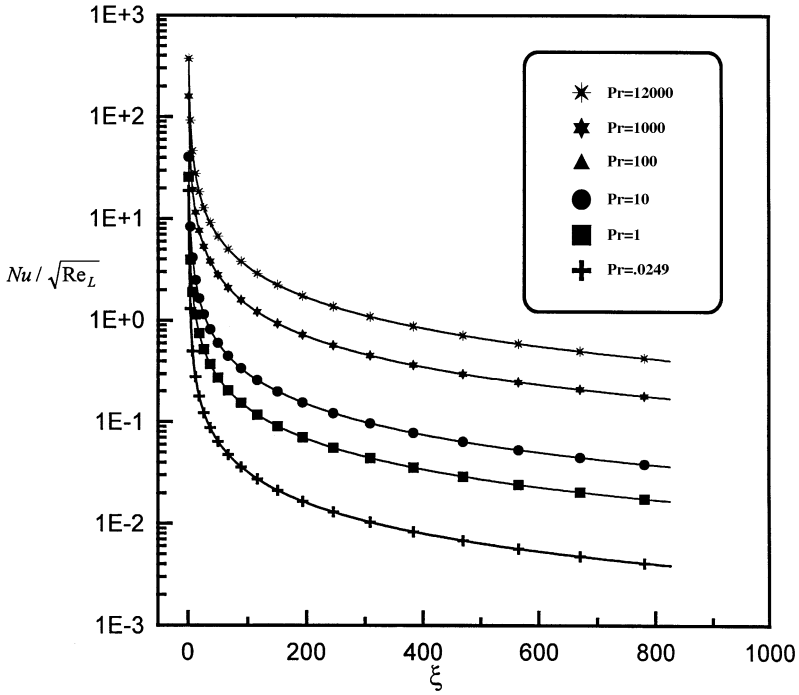

Figure 7.
Nusselt number distribution on a flat plate (Re = 0)

the leading edge and asymptote farther downstream. The corresponding distributions for the case of parabolic cylinder ($Re = 100$) are shown in Figure 8. In the vicinity of the leading edge the distributions experience a peak before they start to asymptote downstream. This can be attributed to the fact that at the leading edge the flow is a localized accelerating stagnation point flow (Hieminz flow). This is expected to enhance the mixing action locally and thus leads to higher values of Nusselt number.

To see the effect of the bluntness (i.e. Reynolds number) on Nusselt number distribution, Nusselt number distributions are plotted again for different values of Reynolds number and for $Pr = 1$. This is shown in Figure 9 where it can be noted that these distributions asymptote to the same value far downstream at the region where Blasius flow holds. The bluntness is expected to affect the flow near the leading edge more than that away from it, and this is exactly what Figure 9 displays.

Finally, the behaviour of the average Nusselt number is presented in Figure 10. It is found that the average Nusselt number increases as the Prandtl number increases. This can be attributed to the decreased thickness of the thermal boundary layer associated with the increase in the Prandtl number. On the other hand, bluntness (increase in Re) is found to decrease the average Nusselt number.

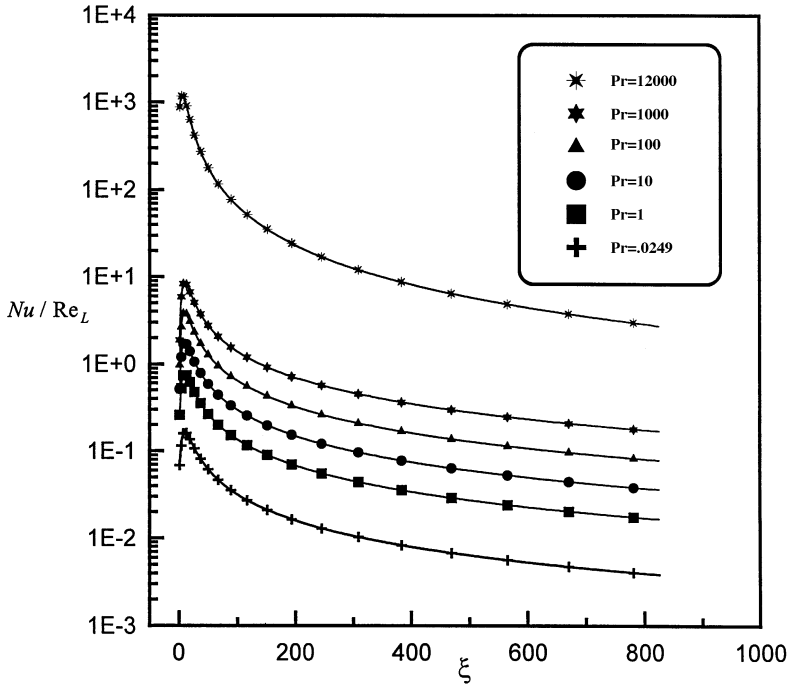

Figure 8.
Nusselt number distribution on a parabolic body (Re = 100)

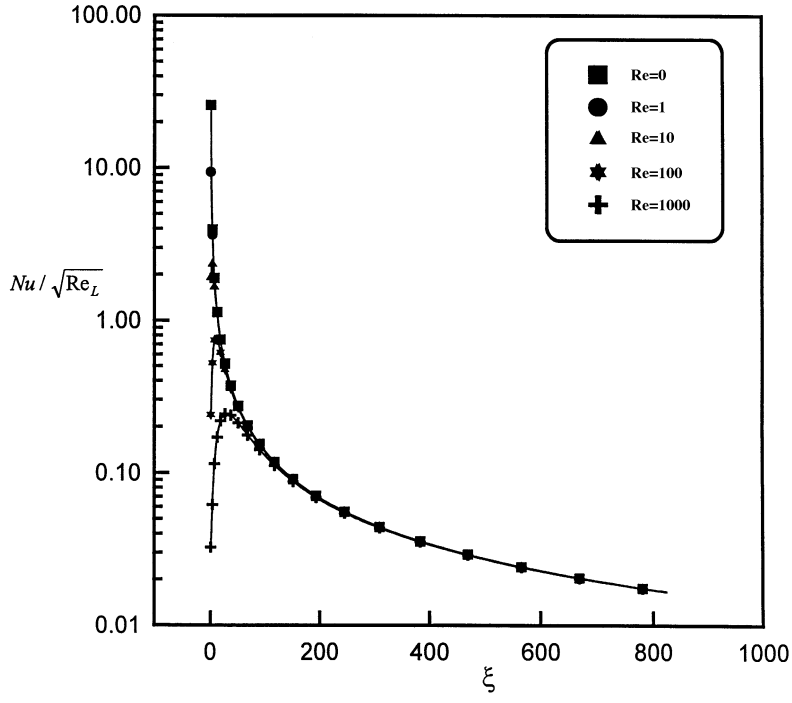

Figure 9.
Effect of bluntness on Nusselt number distribution; Pr = 1

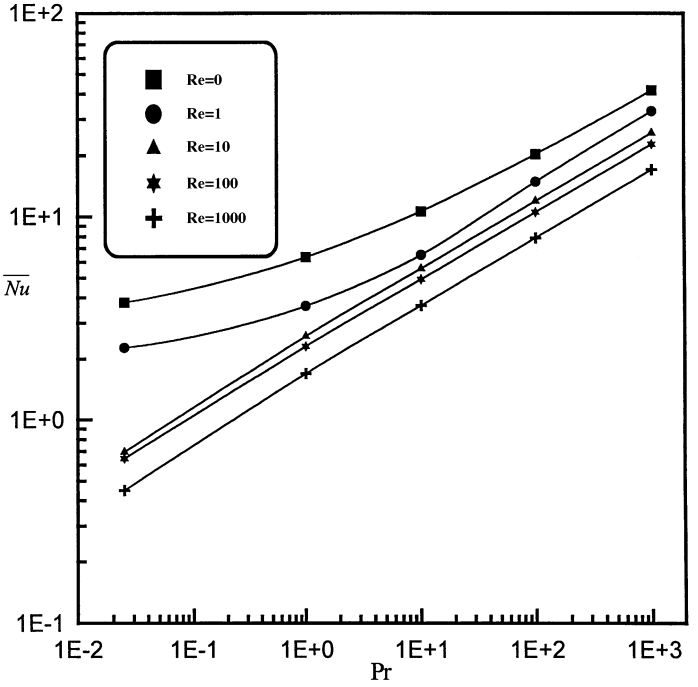

Figure 10.
The behaviour of the average Nusselt number

5. Conclusions

Numerical solutions of the full Navier-Stokes and energy equations that govern the steady two-dimensional symmetric flow past parabolic bodies are presented. A second order accurate finite difference scheme on a non-uniform grid was used to investigate the effect of the problem parameters (e.g. Reynolds number (Re), Prandtl number (Pr)) on the hydrodynamics and heat transfer characteristics of the flow. On the hydrodynamic part, it is found that our results compare very well with those obtained by Davis (1972). This was done to validate our code and results. On the heat transfer part, it is found that the average Nusselt number ($\overline{Nu}$) increases as the Prandtl number (Pr) increases; meanwhile, the average Nusselt number ($\overline{Nu}$) decreases with the increase in the Reynolds number (Re).

References

Anderson, D.A., Tannehill, J.C. and Pletcher, R.H. (1984), *Computational Fluid Mechanics and Heat Transfer*, Hemisphere Publishing Corp.

Botta, E.F.F. and Dijkstra, D. (1970), "An improved numerical solution of the Navier-Stokes equations for laminar flow past a semi-infinite flat plate", Report TW-80, Dept. of Math., University of Groningen.

Botta, E.F.F., Dijkstra, D. and Veldman, A.E.P. (1972), "The numerical solution for Navier-Stokes equations for laminar incompressible flow past a parabolic cylinder", *Journal of Engineering Mathematics*, Vol. 6 No. 1, pp. 63-81.

Davis, R.T. (1967), "Laminar incompressible flow past a semi-infinite flat plate", *Journal of Fluid Mechanics*, Vol. 27, Part 3, pp. 691-704.

Davis, R.T. (1972), "Numerical solution of Navier-Stokes equations for symmetric laminar incompressible flow past a parabola", *Journal of Fluid Mechanics*, Vol. 51, pp. 417-33.

Dennis, S.C.R. and Walsh, J.D. (1971), "Numerical solution for steady symmetric flow past a parabolic cylinder in uniform stream flow", *Journal of Fluid Mechanics*, Vol. 50, pp. 801-14.

Haddad, O.M. (1995), "Numerical study of leading edge receptivity over parabolic bodies", PhD thesis, Illinois Institute of Technology, Chicago, IL.

Haddad, O.M. and Corke, Th. (1998), "Numerical study of leading-edge receptivity on parabolic bodies to freestream acoustic disturbance", *Journal of Fluid Mechanics*, Vol. 368, pp. 1-26.

Maqableh, A.M. (1997), "Flow and heat transfer characteristics for laminar flow over parabolic bodies", MSc thesis, Jordan University of Science and Technology, Irbid, Jordan.

Schlichting, H. (1979), *Boundary Layer Theory*, 7th ed., translated by J. Kestin, McGraw-Hill.

Van De Vooren, A.I. and Dijkstra, D. (1970), "The Navier-Stokes solution for laminar flow past a semi-infinite flat plate", *Journal of Engineering Mathematics*, Vol. 4 No. 4, pp. 9-27.